Cognitive Neurodynamics (2023) 17:755–766
https://doi.org/10.1007/s11571-022-09866-3

RESEARCH ARTICLE

Extreme multistability and phase synchronization in a heterogeneous bi-neuron Rulkov network with memristive electromagnetic induction

Quan Xu[1] · Tong Liu[1] · Shoukui Ding[1] · Han Bao[1] · Ze Li[1] · Bei Chen[1]

Received: 18 June 2022 / Revised: 13 July 2022 / Accepted: 18 July 2022 / Published online: 6 August 2022

Abstract

Memristive electromagnetic induction effect has been widely explored in bi-neuron network with homogeneous neurons, but rarely in bi-neuron network with heterogeneous ones. This paper builds a bi-neuron network by coupling heterogeneous Rulkov neurons with memristor and investigates the memristive electromagnetic induction effect. Theoretical analysis discloses that the bi-neuron network possesses a line equilibrium state and its stability depends on the memristor coupling strength and initial condition. That is, the stability of the line equilibrium state has a transition between unstable saddle-focus and stable node-focus via Hopf bifurcation. By employing parameters located in the stable node-focus region, dynamical behaviors related to the memristor coupling strength and initial conditions are revealed by Julia- and MATLAB-based multiple numerical tools. Numerical results demonstrate that the proposed heterogeneous bi-neuron Rulkov network can generate point attractor, period, chaos, chaos crisis, and period-doubling bifurcation. Note that extreme multistability are disclosed with respect to initial conditions of memristor and gated ion concentration. Coexisting infinitely multiple firing patterns of periodic firing patterns with different periodicities and chaotic firing patterns for different memristor initial conditions are demonstrated by phase portrait and time-domain waveform. Besides, the phase synchronization related to the memristor coupling strength and its initial condition is explored, which suggests that the two heterogeneous neurons become phase synchronization with large memristor coupling strength and initial condition. This also reflects that the plasticity of memristor synapse enables adaptive regulation in keeping energy balance between the neurons. What's more, MCU-based hardware experiments are executed to further confirm the numerical simulations.

Keywords Extreme multistability · Phase synchronization · Memristive electromagnetic induction · Heterogeneous bi-neuron network

Introduction

The brain was known as a heterogeneous structure, leading to the huge diversity in the brain (Gjorgieva et al. 2016). In the recent past, the heterogeneity was considered by employing each neuron an individual membrane, synaptic time constant, and initial conditions in artificial neural network (Duarte and Morrison 2019; Lengler et al. 2013; Padmanabhan and Urban 2010). It has been declared that these heterogeneities can improve the task performance in promoting robust learning (Perez-Nieves et al. 2021) and neural coding (Sachdeva et al. 2020). Except the aforementioned researches initiated in network learning and coding issues, the heterogeneous coupling between neurons should be taken into account in exploring neuron-based small network dynamics. Thus, a heterogeneous bi-neuron Rulkov network is considered in this paper, and then the dynamical behaviors in the network is explored to solidify the ground work in solving complex information tasks under natural environment.

To date, numerous neuron models have been raised to uncover the firing patterns in biological neurons, i.e. Chay model (Chay 1985; Xu et al. 2020a), Hodgkin-Huxley model (Hodgkin and Huxley 1990; Xu et al. 2017), Hindmarsh-Rose model (Gu et al. 2014; Yang and Liao 2019), Morris-Lecar model (Morris and Lecar 1981; Wu et al. 2014), FitzHugh-Nagumo model (FitzHugh 1961),

✉ Bei Chen
chenbei@cczu.edu.cn

[1] School of Microelectronics and Control Engineering, Changzhou University, Changzhou 213164, China

and Rulkov model (Elson et al. 1998; Li et al. 2021a), just to mentioned a few. Up to now, sufficient progress of the coupling dynamics in neuron-based small networks has been achieved. The gap junction (Pal et al. 2020), linear couplers (Shim and Husbands 2018; Wang et al. 2021; Semenov and Fradkov 2021), chemical connections (Bahramian et al. 2021), and blinking coupling (Parastesh et al. 2022) were employed to construct the small networks. Synchronization, a special kind of coupling dynamics, has immersed great concern and investigated in these small networks. It is very interesting that blinking coupling can enhance network synchronization in comparison with the single-variable coupling and the synchronization can be easily achieved by a well-defined blinking period (Parastesh et al. 2022). Also, analytical calculation for sufficient condition for the emergence of the static synchronization state was reported in (Sar et al. 2022).

Besides, the electric field coupling method utilizing capacitor (Liu et al. 2019) and electromagnetic coupling method employing memristor (Zhang and Liao 2017; Bao et al. 2019; Xu and Zhu 2020) were presented. In these literatures, synchronous behaviors, multiple vibrational resonances, chaotic dynamics, multistability, and collective behaviors were revealed in theoretical and numerical surveys. Among these coupling methods, the memristor coupling method has its own feature, since the memristor is a special nonlinearity owning internal state. What's more, a flux-controlled memristor has been utilized to characterize the electromagnetic induction induced by membrane potential of a single neuron (Yang et al. 2021) or by the difference between membrane potentials of two adjacent neurons (Xu and Zhu 2020). The physical mechanism of memristive electromagnetic induction in biology has been declared by Ma et al. in (Lv and Ma 2016). It has been declared that memristive synapse has similar field effect and biophysical properties as the chemical synapse (Wu et al. 2022). In other words, memristive synapse can trigger similar neuron electrical activities as activated by chemical synapse. What's more, memristive synapse has adaptive characteristic due to the plasticity of memristor, which is helpful in achieving fast energy balance between coupling neurons (Xie et al. 2022). In this paper, a flux-controlled memristor is employed as a coupled synapse to depict the electromagnetic induction induced by membrane potentials difference between the two heterogeneous Rulkov neurons.

No matter which coupling methods they employed, most of these neuron-based small networks were composited by homogeneous neurons. Various types of synchronization can be easily achieved in these networks, such as complete synchronization (Bao et al. 2020; Wouapi et al. 2021; Mehrabbeik et al. 2021), phase synchronization (Zhang et al. 2020; Ma et al. 2017), and lag synchronization (Wang and Shi 2012). What's more, complete synchronization induced by pulse (Nakamura and Tateno 2019) and phase synchronization (De and Balakrishnan 2020; Yao et al. 2021; Li et al. 2021b) have also been explored in non-identical neuron-based networks. It has been acknowledged that complete synchronization is hard to realize without externally applied stimulus in heterogeneous neuron-based network. Thus, only the phase synchronization in the proposed heterogeneous bi-neuron Rulkov network is investigated in this paper. Besides, the proposed bi-neuron network can be regarded as a memristive system possessing a line equilibrium state. That's fully resulted by the involvement of an ideal memristor (Bao et al. 2019b). The stability of the line equilibrium state is really associated to the initial condition of the memristor (Xu et al. 2021b; An and Qiao 2021). This might trigger extreme multistability with coexisting infinitely multiple firing patterns. To our knowledge, such extreme multistability has not yet been raised in bi-neuron network with electromagnetic induction. The contributions and novelty can be summarized as follows. 1) To better characterize electromagnetic induction effects between heterogeneous neurons, a memristor synapse-coupled Rulkov bi-neuron network with line equilibrium state is presented. 2) Extreme multistability with coexisting infinitely multiple firing patterns are disclosed. 3) A MCU-based experimental measurement platform is built and hardware experiments are executed to confirm the generation of coexisting infinitely multiple firing patterns.

The rest of this paper is arranged as follows. A memristor synapse-coupled Rulkov bi-neuron network is proposed and then its equilibrium state stability is explored. Dynamical behavior related to memristor synapse is studied and dynamics related to the initial conditions of gated ion concentrations are disclosed. What's more, the numerical explorations of phase synchronization are depicted. Furthermore, MCU-based experimental measurements are executed to confirm the numerical simulations. Finally, our conclusion is summarized.

Memristor synapse-coupled Rulkov bi-neuron network

To more efficiently reflect the continuous dynamical evolution process of a biological neuron, a two-dimensional (2D) continuous Rulkov model is built (Xu et al. 2021b). The 2D continuous Rulkov model has a simple mathematical expression and can generate periodic spiking behavior. To explore the electromagnetic induction effects between two such neurons, a memristor synapse-coupled heterogeneous bi-neuron Rulkov network is built as

$$\begin{cases} \dfrac{dx_1}{dt} = \dfrac{\alpha_1}{1+x_1^2} - x_1 + y_1 + kW(\varphi)(x_1 - x_2), \\ \dfrac{dy_1}{dt} = -\sigma x_1 - \beta, \\ \dfrac{dx_2}{dt} = \dfrac{\alpha_2}{1+x_2^2} - x_2 + y_2 - kW(\varphi)(x_1 - x_2), \\ \dfrac{dy_2}{dt} = -\sigma x_2 - \beta, \\ \dfrac{d\varphi}{dt} = x_1 - x_2, \end{cases} \tag{1}$$

where x_1 and x_2 are the fast variables representing the membrane potentials of the two neurons. y_1 and y_2 are two slow variables standing for the gated ion concentrations on membrane. $kW(\varphi)(x_1 - x_2)$ stands for the electromagnetic induction current induced by the difference of membrane potentials x_1 and x_2, where k is the coupling strength and $W(\varphi)$ is the memductance of the memristor controlled by its inner state variable φ. α_1, α_2, β, and σ are four model parameters with non-negative values. In particular, σ is the changing rate of gated ion concentration. The model parameter β stands for the externally applied influence. Herein, we set $\beta = 0$ without the consideration of externally applied influence. In following sections, we determine the model parameters $\alpha_1 = 12$, $\alpha_2 = 6$, $\sigma = 6$, and select k as adjustable parameter. Herein, $\alpha_1 \neq \alpha_2$ means that the two neurons are heterogeneous.

Setting the left side of (1) to 0, the equilibrium state can be analytically calculated as

$$\mathbf{E} = (\overline{x}_1, \overline{y}_1, \overline{x}_2, \overline{y}_2, \overline{\varphi}) = (0, -\alpha_1, 0, -\alpha_2, c), \tag{2}$$

where c is an arbitrary constant corresponding to the initial position on the φ-axis. This declares that (1) has a line equilibrium state along the memristor state variable axis.

The stability of the equilibrium state is characterized by the characteristic roots of Jacobian matrix for a dynamical system at that equilibrium state. The Jacobian matrix of (1) at $\boldsymbol{E}$ is obtained as

$$\mathrm{J}_{\mathbf{E}} = \begin{bmatrix} kc-1 & 1 & -kc & 0 & 0 \\ -\sigma & 0 & 0 & 0 & 0 \\ -kc & 0 & kc-1 & 1 & 0 \\ 0 & 0 & -\sigma & 0 & 0 \\ 1 & 0 & -1 & 0 & 0 \end{bmatrix}. \tag{3}$$

Then the characteristic polynomial equation is calculated as

$$\det(\mathbf{1}\lambda - \boldsymbol{J_E}) = \lambda(\lambda^2 + \lambda + \sigma)[\lambda^2 + (1 - 2kc)\lambda + \sigma] = 0. \tag{4}$$

The characteristic roots of Eq. (4) determine the stability of the line equilibrium state. The parameters k, c, and σ restrict the characteristic roots of Eq. (4). Herein, we mainly consider the electromagnetic induction effect related to the memristor synapse parameters k and c with $\sigma = 6$. Model (1) always has a zero-root due to the existence of ideal memristor. The non-zero characteristic roots and stability types for different parameter range of kc are listed in Table 1, where USF, SNF, and HBP stand for unstable saddle-focus, stable node-focus, and Hopf bifurcation point, respectively. Then, the stability distributions of equilibrium point $\boldsymbol{E}$ in the $c - k$ parameters plane are drawn as shown in Fig. 1. The parameters k and c are respectively varied in [0, 0.8] and [− 6, 6]. The lines colored in red, black, and blue represent the boundaries of different stability regions, respectively. The parameters k and c within the magenta rectangle plotted in dash-line, i.e. k [0.45, 0.7] and c [− 0.1, 0.5], are considered to explore the electromagnetic induction effect in the following sections. The equilibrium state is a stable node-focus in the parameter ranges, which implies that the firing patterns generated in model (1) might be hidden (Bao et al. 2019b, Xu et al. 2021a). The line equilibrium state is not always stable in the full parameter plane. With those considerations, the generated firing pattern in model (1) might be named as local hidden dynamics. This is an open issue for the potential researchers.

Dynamics related to memristor synapse

Julia-based ODE45 algorithm is employed to simulate the two-dimensional (2D) bifurcation plots. The fixed time-step and time-interval are set to 0.01 s and [3 ks, 4 ks] respectively. The Wolf's Jacobian-based method with fixed time-step 0.1 s and time-end 20 ks is utilized for computing the finite-time Lyapunov exponent.

The initial conditions $[x_1(0), y_1(0), x_2(0), y_1(0), \varphi(0)] = [10^{-9}, 0, 10^{-9}, 0, \varphi(0)]$ are utilized to explore the dynamical effect related to the memristor synapse. The coupling strength k and memristor initial condition $\varphi(0)$ are adjusted in the regions [0.45, 0.7] and [− 0.1, 0.5] respectively. The 2D bifurcation plot and dynamical map are figured out in Fig. 2. The 2D bifurcation plot is plotted by inspecting the periodicity of membrane potential x_1 and dynamical map is described by the largest Lyapunov exponent (LLE). In Fig. 2a, the different colors on the color bar are utilized to distinguish different firing patterns. The marks PA, CH, and P1 ∼ P8 stand for point attractor, chaotic behavior, and period-1 to period-8, respectively. The 2D bifurcation plot demonstrates that the firing patterns generated in model (1) are very associated to the coupling strength and memristor initial condition. The 2D bifurcation plot mainly has a banded structure and some dynamical behaviors have narrow parameter ranges. These narrow ranges for the corresponding dynamical behaviors are hardly visible, but they are confirmed by checking the

Table 1 Characteristic roots and stability types for different parameters

Parameter range	Non-zero characteristic roots	Stability types
$kc \geq \frac{1+2\sqrt{6}}{2}$	Two positive real roots, and a pair of conjugate complex roots with negative real part	USF
$\frac{1}{2} < kc < \frac{1+2\sqrt{6}}{2}$	two pairs of conjugate complex roots With opposite real parts	USF
$kc = \frac{1}{2}$	A pair of conjugate complex roots with negative real part, and a pair of pure imaginary roots	HBP
$\frac{1-2\sqrt{6}}{2} < kc < \frac{1}{2}$	Two pairs of conjugate complex roots with negative real parts	SNF
$kc \leq \frac{1-2\sqrt{6}}{2}$	Two negative real roots, and a pair of conjugate complex roots with negative real part	SNF

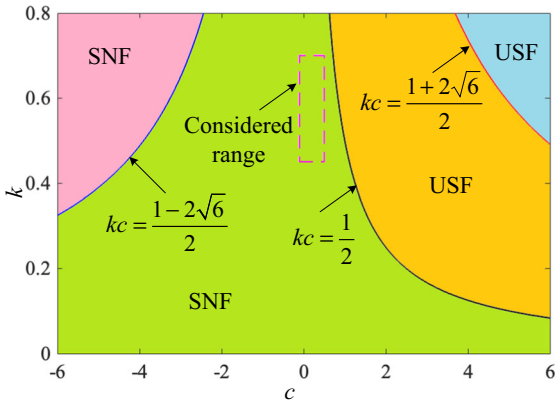

Fig. 1 Stability distributions in the c–k parameters plane for parameters $\alpha_1 = 12$, $\alpha_2 = 6$, $\sigma = 6$, and $\beta = 0$ in model (1) (Color figure online)

data for bifurcation plot. In Fig. 2b, the red regions with positive LLE stand for chaotic behaviors, the black regions with LLE = 0 present periodic behaviors, and the grey region with LLE < 0 stands for point attractor. Figure 2b declares that the dynamical map further confirms the firing patterns revealed by 2D bifurcation plot.

To further uncover the bifurcation behavior with respect to the coupling strength k and memristor initial condition $\varphi(0)$, MATLAB-based 1D bifurcation plot and Lyapunov exponents (LEs) are numerically simulated. When the coupling strength k increases in the interval [0.45, 0.7], the 1D bifurcation plot of the local maxima of x_1 (denoted as $x_{1\max}$) and LEs are figured out in Fig. 3a, where the trajectories are triggered by $[x_1(0), y_1(0), x_2(0), y_2(0), \varphi(0)] = [10^{-9}, 0, 10^{-9}, 0, 0]$. When gradually increasing k from 0.45, the trajectory of model (1) starts with point attractor and then jumps to period-1 at $k = 0.4886$. The trajectory runs into period-2, period-4, and period-8 at $k = 0.5176$, 0.5236, and 0.5246 via period-doubling bifurcations, respectively. Then the trajectory enters into chaos via further period-doubling bifurcations and then drops to period-3 due to the occurrence of chaos crisis at $k = 0.5280$. Thereafter, the trajectory goes to chaos again via period-doubling bifurcation route and drops to periodic behavior. The 1D bifurcation plot demonstrates that this process happens many times until $k = 0.6802$. Afterwards, the trajectory of model (1) runs in period-1. The first two LEs are plotted in the bottom of Fig. 3a, which can effectively confirm the dynamics evolution with respect to the coupling strength k. When the memristor initial condition $\varphi(0)$ increases from -0.1 to 0.5 with $k = 0.5$, the 1D bifurcation plot and LEs are potted in Fig. 3b. The bifurcation behaviors with respect to the memristor initial condition $\varphi(0)$ are similar to these with respect to coupling strength k.

The numerical simulations in Fig. 3 demonstrate that model (1) can produce rich dynamical behaviors, including point attractor, period, chaos, chaos crisis, and period-doubling bifurcation with the adjustments of k and $\varphi(0)$. Notably, the occurrence of period-doubling bifurcation routes with respect to memristor initial condition declares the existence of coexisting infinitely multiple firing patterns. From the biological point of view, these results can explain the appearance of coexisting firing patterns in neurophysiological experiments for biological systems since they display functional flexibility (Pisarchik and

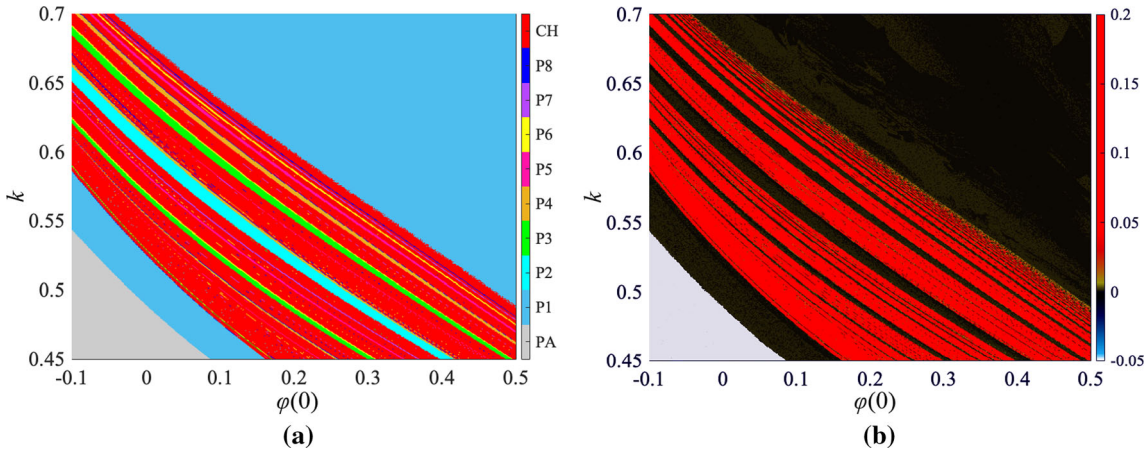

Fig. 2 The 2D bifurcation behaviors in $\varphi(0)$–k hybrid parameter plane for parameters $\alpha_1 = 12$, $\alpha_2 = 6$, $\sigma = 6$, and initial conditions $[x_1(0), y_1(0), x_2(0), y_1(0), \varphi(0)] = [10^{-9}, 0, 10.^{-9}, 0, \varphi(0)]$. **a** The 2D bifurcation plot, **b** dynamical map (Color figure online)

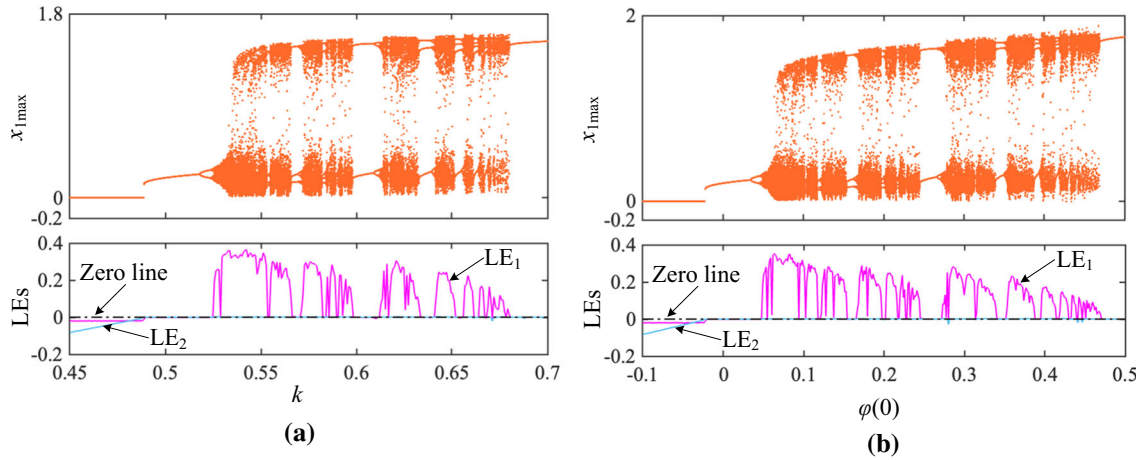

Fig. 3 The 1D bifurcation behaviors of bifurcation plot (up) and finite-time LEs (bottom) with respect to k and $\varphi(0)$ respectively. **a** Coupling strength k increasing from 0.45 to 0.7 with $\alpha_1 = 12$, $\alpha_2 = 6$, $\sigma = 6$, and initial conditions $[x_1(0), y_1(0), x_2(0), y_1(0), \varphi(0)] = [10^{-9}, 0, 10^{-9}, 0, 0]$, **b** memristor initial condition $\varphi(0)$ increasing from -0.1 to 0.5 with $\alpha_1 = 12$, $\alpha_2 = 6$, $\sigma = 6$, $k = 0.5$, and initial conditions $[x_1(0), y_1(0), x_2(0), y_1(0), \varphi(0)] = [10^{-9}, 0, 10.^{-9}, 0, \varphi(0)]$ (Color figure online)

Feudel, 2014; Pisarchik et al. 2018). On the other hand, these results reflect that extreme multistability with coexisting infinitely multiple firing patterns in biological neurons can be reproduced by considering the participation of electromagnetic induction.

To demonstrate the coexisting infinitely multiple firing patterns, the phase portraits in the x_1–x_2 and y_1–y_2 phase planes and the time-domain waveforms of membrane potentials x_1 and x_2 for different initial conditions are numerically simulated as shown in Fig. 4. The time-step 0.01 s and time interval [3.9 ks, 4 ks] are utilized in calculating the phase portrait and time-domain waveform. Herein, the parameters $\alpha_1 = 12$, $\alpha_2 = 6$, $\sigma = 6$, and $k = 0.5$ and initial conditions $[x_1(0), y_1(0), x_2(0), y_2(0), \varphi(0)] = [10^{-9}, 0, 10^{-9}, 0, \varphi(0)]$ with adjustable $\varphi(0)$ are exhibited as an example. Note that only some examples for different $\varphi(0)$ are used to demonstrate the coexisting infinitely multiple firing patterns, since it is impossible to exhaustive them all. It is demonstrated that model (1) can truly trigger coexisting infinitely multiple firing patterns. The amplitudes of firing patterns for the two neurons are in the same scale with small $\varphi(0)$, i.e. $\varphi(0) \leq 0.0661$, but they are in different orders for $\varphi(0)$ bigger than the value. What's more, the dynamical behaviors for the two neurons are different in some regions of $\varphi(0)$, just like the cases shown in Fig. 4d and f. Therefore, the selection of the expected firing patterns can be effectively realized by controlling the memristor initial condition.

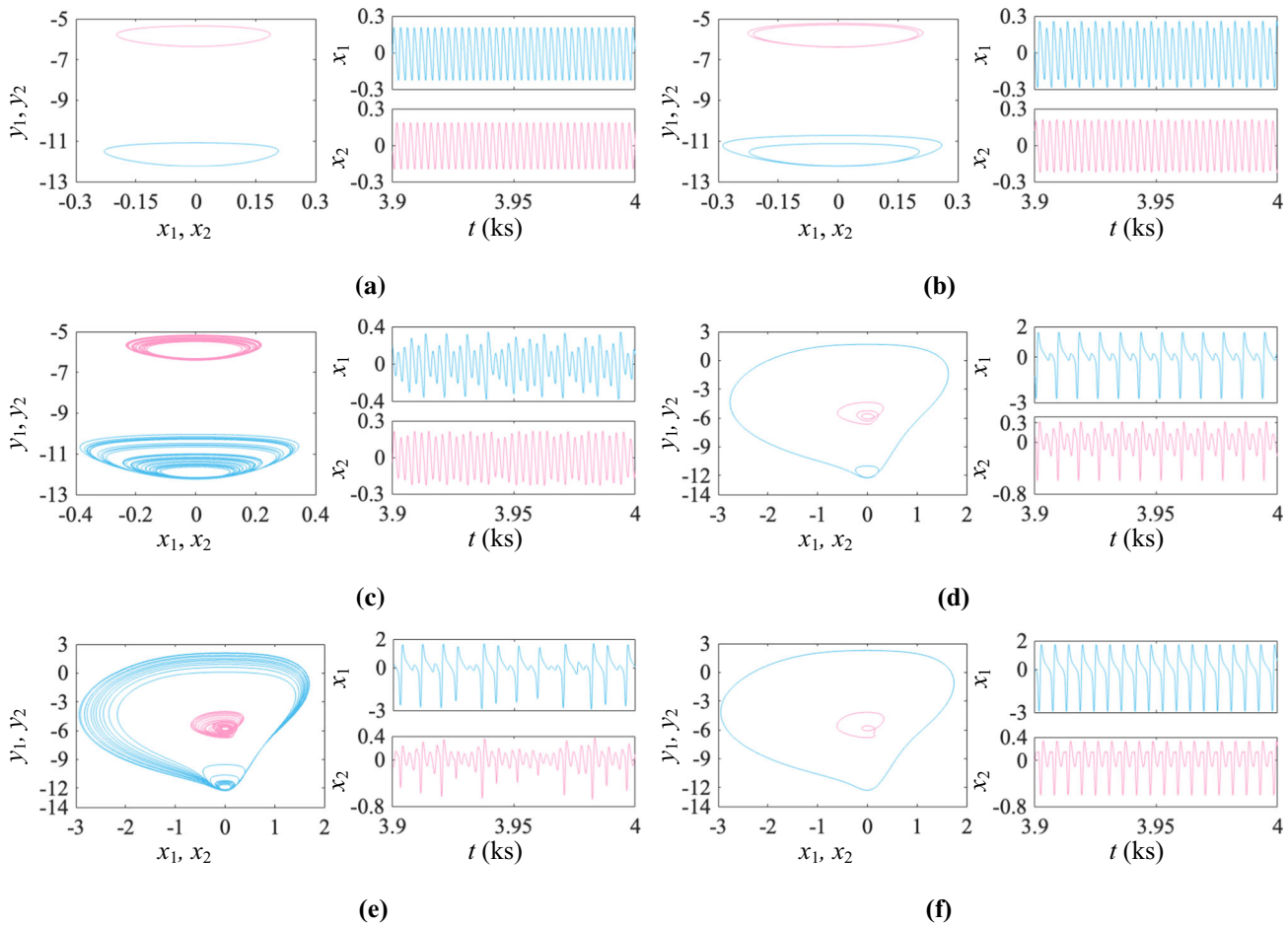

Fig. 4 Phase portrait (left) and time-domain waveforms (right) for different initial conditions $[x_1(0), y_1(0), x_2(0), y_2(0), \varphi(0)] = [10^{-9}, 0, 10.^{-9}, 0, \varphi(0)]$ with $\alpha_1 = 12$, $\alpha_2 = 6$, $\sigma = 6$, and $k = 0.5$. **a** Period-1 firing patterns for $\varphi(0) = 0.01$, **b** period-2 firing patterns for $\varphi(0) = 0.04$, **c** chaotic firing patterns for $\varphi(0) = 0.06$, **d** period-2 and period-3 firing patterns for $\varphi(0) = 0.25$, **e** chaotic firing patterns for $\varphi(0) = 0.30$, **f** period-1 and period-2 firing patterns for $\varphi(0) = 0.48$ (Color figure online)

Dynamics related to the initial conditions of gated ion concentrations

In this section, coexisting infinitely multiple firing patterns depend on the initial conditions of gated ion concentrations are explored. The control parameters are employed as the typical ones. The initial conditions $[x_1(0), y_1(0), x_2(0), y_2(0), \varphi(0)] = [10^{-9}, y_1(0), 10^{-9}, y_2(0), 0]$ are assigned, and $y_1(0)$ and $y_2(0)$ are adjusted in the regions $[-0.5, 3]$ and $[-3, 0.5]$ respectively. Figure 5 shows the local attraction basins (Yu et al. 2022) and dynamical maps in the $y_1(0)$–$y_2(0)$ initial condition plane. The marks UH, PA, CH, and P1 $\sim$ P8 on the color bar stand for unbounded behavior, point attractor, chaotic behavior, and period-1 to period-8, respectively. The local attraction basin demonstrates that the rich firing patterns are triggered by initial conditions of gated ion concentrations. What's more, the local attraction basin also has a banded structure and some dynamical behaviors have narrow parameter ranges as shown in Fig. 5a. In Fig. 5b, the red regions with LLE > 0, the black regions with LLE $= 0$, the grey region with LLE < 0, and the white region with no LE stand for chaotic behaviors, periodic behaviors, point attractor, and unbounded behavior in the dynamical map, respectively. The dynamical map can further confirm the dynamical behaviors revealed by the local attraction basin. Therefore, the memristor synapse-coupled heterogeneous bi-neuron Rulkov network not only can generate coexisting infinitely multiple firing patterns depending on the memristor initial condition, but also can generate these behaviors associating to the initial conditions of gated ion concentrations.

As predicted in Fig. 5, coexisting infinitely multiple firing patterns are triggered by the initial conditions $y_1(0)$ and $y_2(0)$. The 1D bifurcation plots and first two finite-time LEs are depicted in Fig. 6 to reveal the bifurcation behaviors. The initial conditions $[x_1(0), y_1(0), x_2(0), y_2(0), \varphi(0)] = [10^{-9}, y_1(0), 10^{-9}, 0, 0]$ and $[10^{-9}, 0, 10^{-9}, y_2(0), 0]$ are employed in Fig. 6a and b respectively. The 1D

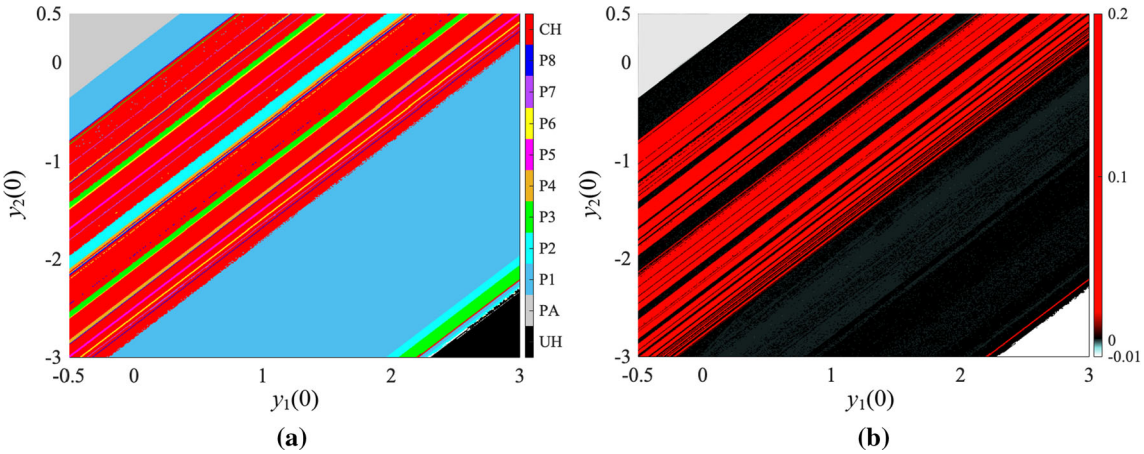

Fig. 5 Local attraction basin and dynamical map in $y_1(0)$– $y_2(0)$ initial condition plane with $\alpha_1 = 12$, $\alpha_2 = 6$, $\sigma = 6$, $k = 0.5$, and initial conditions $[x_1(0), y_1(0), x_2(0), y_2(0), \varphi(0)] = [10^{-9}, y_1(0), 10.^{-9}, y_2(0), 0]$. **a** Local attraction basin, **b** dynamical map (Color figure online)

bifurcation plots of the local maxima of x_1 (denoted as $x_{1\max}$) and x_2 (denoted as $x_{2\max}$) are figured out in the up and middle. The first two finite-time LEs are plotted in the bottom. With the initial conditions $y_1(0)$ and $y_2(0)$ varying in [− 0.5, 3] and [− 3, 0.5], the bifurcation behaviors are similar with those revealed in Fig. 3. What's more, model (1) can produce rich dynamical behaviors such as period, chaos, chaos crisis, and period-doubling bifurcation. Note that the local maxima amplitudes of x_1 and x_2 are different. This reflects that firing patterns of the two neurons are running in different dynamic amplitudes. What's more, extreme multistability is triggered since the existence of period-doubling bifurcation or reverse period-doubling bifurcation with respect to initial condition (Bao et al. 2016).

Phase synchronization

Unlike the complete synchronization, phase synchronization has been revealed in non-identical coupled neuron model described by the same mathematical form (Wang et al. 2010) or described by completely different coupled neurons (Yao et al. 2021; Li et al. 2021b). In these literatures, the burst phase is defined as

$$\theta(t) = 2n\pi + 2\pi\frac{t - t_n}{t_{n+1} - t_n}, (t_n < t < t_{n+1}). \quad (5)$$

where t_n is the nth burst emerging time. $t_{n+1} - t_n$ is time interval of the nth burst. The phase increases 2π accompanying with each generated burst. Thus, the phase synchronization can be identified by detecting the phase difference

$$|\Delta\theta(t)| = |\theta_1(t) - \theta_2(t)|, \quad (6)$$

where the absolute value is utilized to restrict the phase difference as positive values and the phase synchronization is achieved with its value tending to a constant.

To illustrate the phase synchronization behavior in bi-neuron network (1), the memristor initial condition $\varphi(0)$ and coupling strength k are adjusted in the regions [− 0.8, 0.8] and [0.1, 0.8] respectively. In the $\varphi(0) - k$ hybrid parameter plane, the phase synchronization behavior is depicted by checking the phase difference $|\Delta\theta(t)|$ versus time t. In Fig. 7a, the different regions padded by different colors stand for different phase synchronization behaviors, i.e. red for complete phase synchronization, light-blue for finite-time phase synchronization, and yellow for phase non-synchronization. Note that the stability point behavior of the two neurons are marked as phase non-synchronization. The two heterogeneous neurons become complete phase synchronization for the memristor coupling strength and initial condition in the red regions.

To further demonstrated the different phase synchronization behaviors, the phase difference with respect to time are plotted for four sets of parameters belonging to different regions as shown in Fig. 7b. When $k = 0.5$ and $\varphi(0) = -0.3$, the phase difference equals to zero and then rises monotonically. This manifests that two neurons are finite-time phase synchronization. When $k = 0.5$ and $\varphi(0) = 0.5$, the phase difference tends to infinite, which declares that two neurons are phase non-synchronization. Whereas for $k = 0.5$ and $\varphi(0) = 0.01$, as well as $k = 0.8$ and $\varphi(0) = 0.8$, the phase differences tend to constants representing the achievement of complete phase synchronization. It is revealed that complete phase synchronization and finite-time phase synchronization are found. What's more, complete phase synchronization can be achieved in very short time, which is benefit by the fast energy balance between memristor synapse coupling neurons (Xie et al.

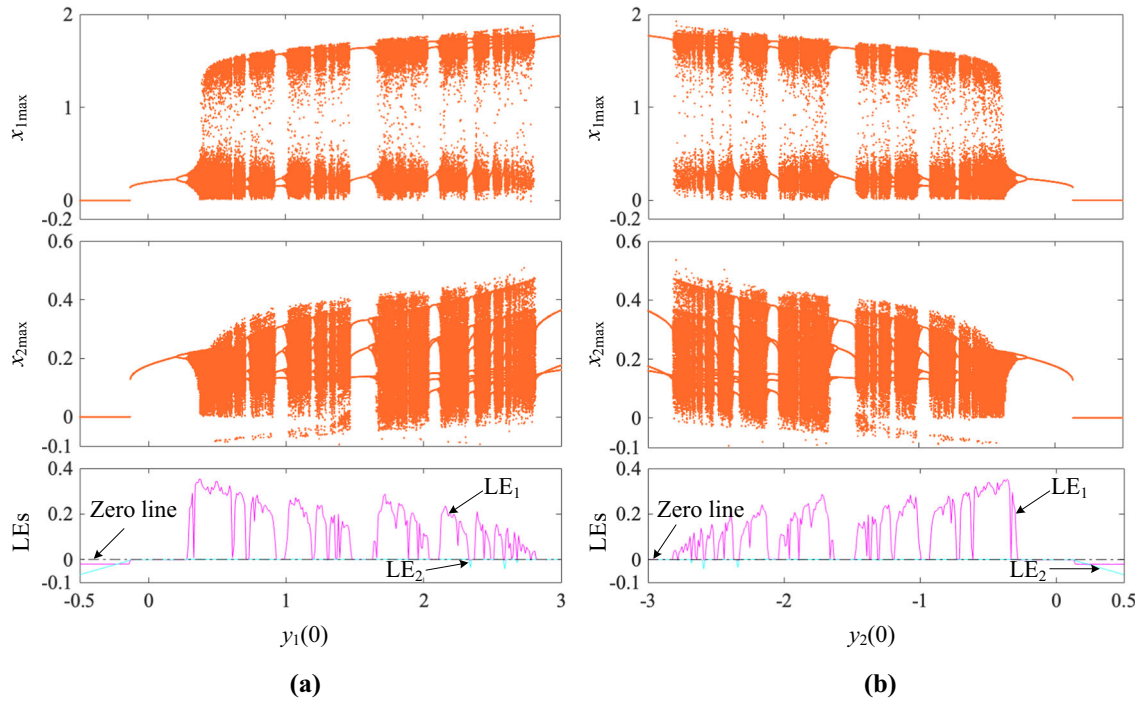

Fig. 6 The 1D bifurcation behaviors of bifurcation plots for the local maxima of x_{1max} and x_{2max} (up and middle) and finite-time LEs (bottom) with the variations of $y_1(0)$ and $y_2(0)$ respectively. The other parameters are $\alpha_1 = 12$, $\alpha_2 = 6$, $\sigma = 6$, $k = 0.5$. **a** Initial condition $y_1(0)$ increasing from -0.5 to3 with initial conditons $[x_1(0), y_1(0), x_2(0), y_2(0), \varphi(0)] = [10^{-9}, y_1(0), 10^{-9}, 0, 0]$, **b** initial condition $y_2(0)$ increasing from -3 to 0.5 with initial conditions $[x_1(0), y_1(0), x_2(0), y_2(0), \varphi(0)] = [10^{-9}, 0, 10.^{-9}, y_2(0), 0]$ (Color figure online)

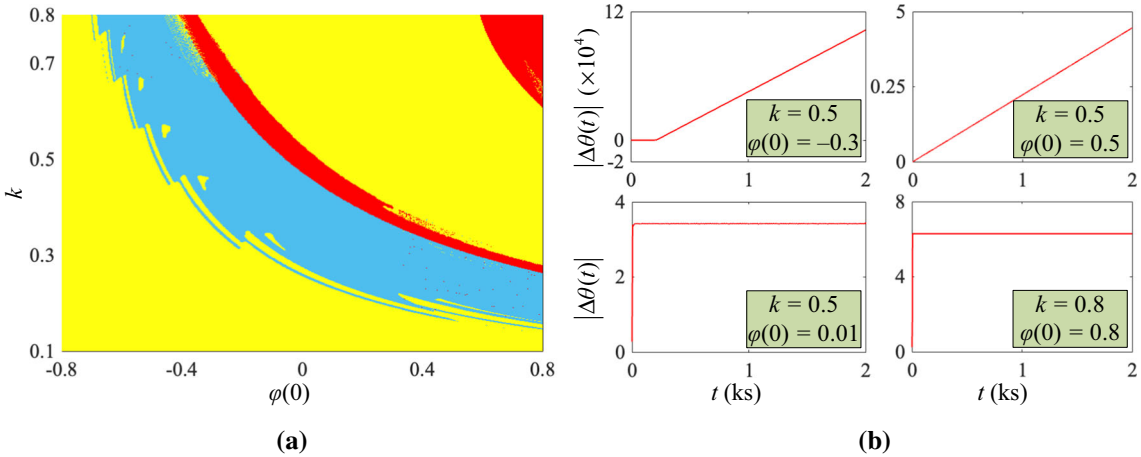

Fig. 7 Phase synchronization behavior explored by checking the phase difference with respect to memritor initial $\varphi(0)$ and coupling strength k. The other parameters are fixed as $\alpha_1 = 12$, $\alpha_2 = 6$, $\sigma = 6$, and initial conditions $[x_1(0), y_1(0), x_2(0), y_2(0), \varphi(0)] = [10^{-9}, 0, 10.^{-9}, 0, \varphi(0)]$. **a** Phase synchronization in the $\varphi(0) - k$ hybrid parameter plane, **b** different phase synchronization behaviors versus time, those are, finite-time phase synchronization (up-left), phase non-synchronization (up-right) and complete phase synchronization (down-left and down-right) (Color figure online)

2022). The plasticity of memristor synapse enables adaptive regulation in keeping energy balance between the neurons (Zhou et al. 2022). Besides, with the memristor synapse connection having adaptive characteristic between the two neurons, the proposed model (1) demonstrates explosive transition (Majhi et al. 2022) to complete phase synchronization as shown in the up of Fig. 7b. Actually, the memristor synapse is a functional connectivity to realize the transformations of energy, matter, or information between the two neurons, which refers to the underlying dynamical processes (Gosak et al. 2022).

MCU-based experimental confirmation

Hardware platform for implementing neuron-based network can obtain real biological system functionalities and widen their engineering application. Herein, a MCU-based hardware platform is developed for implementing the bi-neuron network (1), upon which the experimental measurements are executed to verify the numerical simulations. The hardware platform is mainly built by a 32-bit STM32F407 microcontroller (Bakiri et al. 2018; Njitacke et al. 2021), two 16-bit DAC8563 D/A converters, a DSOX6004A oscilloscope, and other peripheral circuits. The snapshot of the experimental measurement platform for the MCU-based hardware platform is shown in Fig. 8. The 32-bit STM32F407 microcontroller is employed to implement the discrete-time model of (1) obtaining by fourth-order Runge–Kutta algorithm (Xu et al. 2020). The 16-bit DAC8563 D/A converters convert the digital signals to analog voltage ones in the voltage level [0 V, 5 V]. The peripheral circuits realize the voltage level conversion to [− 10 V, 10 V]. Note that the dynamic amplitudes of y_1 and y_2 are out of this range. Thus, they are rescaled to one-tenth with respect to their original ones and then the results are outputted to the connected DSOX6004A oscilloscope.

All the programs are coded in the form of C language compiled in the Keil μVision5 and then downloaded to the MCU. The model parameters and initial conditions are employed as those utilized in Fig. 4. When the power supply is turn on, the phase trajectories can be captured by DSOX6004A oscilloscope in XY mode. Then, time-domain waveforms of the analog voltage signals can be synchronously captured. Note that the outputs of the peripheral circuits are analog voltages V_{x1}, V_{y1}, V_{x2}, and V_{y2} corresponding to the state variables x_1, y_1, x_2, and y_2 in (1), respectively. The experimentally measured results for different memristor initial conditions are captured by screen shot as shown in Fig. 9. For better visualization, the colors for phase trajectories and time-domain waveforms are changed by Photoshop software. It shows that the experimentally measured results are in good agreement with the numerical simulation results as shown in Fig. 4, which indicates the feasibility of the hardware platform for the heterogeneous bi-neuron Rulkov network with memristive electromagnetic induction.

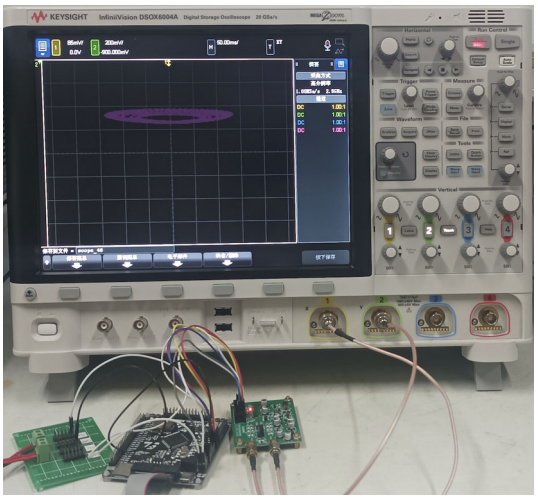

Fig. 8 The snapshot of MCU-based experimental measurement platform (Color figure online)

Conclusion

In this paper, extreme multistability and phase synchronization in a heterogeneous bi-neuron Rulkov network with memristive electromagnetic were numerically and experimentally studied. The bi-neuron network possesses a line equilibrium state located in the memristor inner state axis. The stability of the line equilibrium state really depends on the memristor coupling strength and initial conditions, and there has unstable saddle-focus, stable node-focus, or Hopf bifurcation point. Dynamical behaviors related to the memristor coupling strength and initial conditions were revealed for the parameters located in stable node-focus region. The results demonstrate that rich firing patterns are emerged in the bi-neuron network. Especially, perfect period-doubling bifurcation are generated with respect to the initial conditions of memristor and gated ion concentrations, thereby leading to that the extreme multistability with coexisting infinitely multiple firing patterns are triggered. Moreover, phase synchronization of the bi-neuron network was numerically explored with respect to the memristor coupling strength and initial condition. The numerical results declare that phase synchronization can be achieved with large memristor coupling strength and initial condition, whereas finite-time phase synchronization and phase non-synchronization exist in the other parameters' regions. This is very different from the conditions for complete synchronization in memristor synapse coupled Hindmarsh-Rose bi-neuron network (Bao et al. 2019a) and FitzHugh-Nagumo bi-neuron network (Xu and Zhu 2020). What's more, these numerical results were effectively confirmed by MCU-based experimental measurement. The numerical and experimental explorations can provide insights for understanding the firing patterns in heterogeneous bi-neuron network with memristive electromagnetic induction.

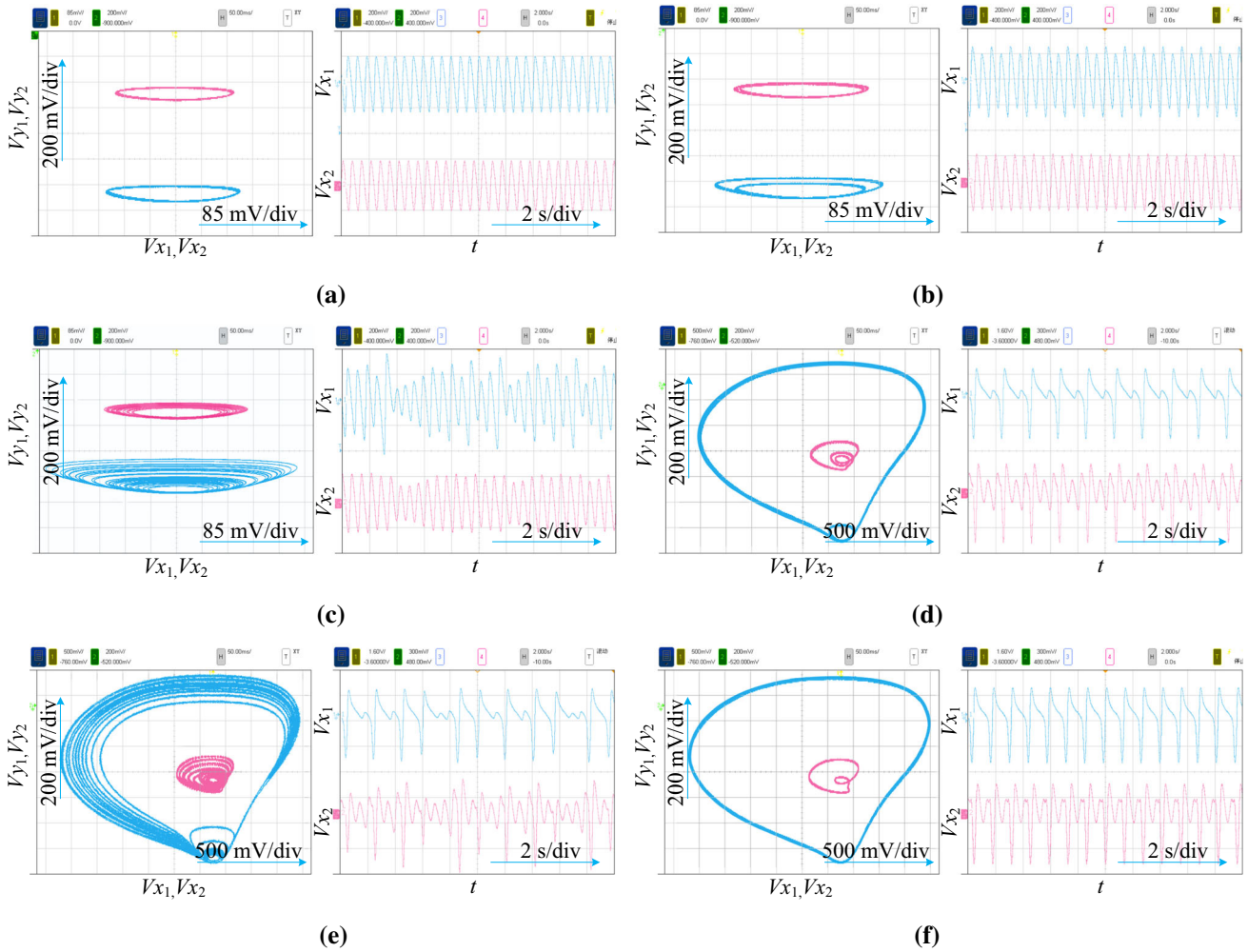

Fig. 9 Experimentally captured phase trajectories in the $V_{x1}-V_{y1}$ and $V_{x2}-V_{y2}$ planes and time-domain waveforms for different initial conditions $[x_1(0), y_1(0), x_2(0), y_2(0), \varphi(0)] = [10^{-9}, 0, 10.^{-9}, 0, \varphi(0)]$. **a** Period-1 firing patterns for $\varphi(0) = 0.01$, **b** period-2 firing patterns for $\varphi(0) = 0.04$, **c** chaotic firing patterns for $\varphi(0) = 0.06$, **d** period-2 and period-3 firing patterns for $\varphi(0) = 0.25$, **e** chaotic firing patterns for $\varphi(0) = 0.30$, **f** period-1 and period-2 firing patterns for $\varphi(0) = 0.48$ (Color figure online)

Acknowledgements This work was supported by the National Natural Science Foundation of China under Grant 12172066, Grant 61801054, and Grant 51777016, the Natural Science Foundation of Jiangsu Province, China, under Grant BK20160282 and Grant BK20210850, the Project 333 of Jiangsu Province, and the Postgraduate Research and Practice Innovation Program of Jiangsu Province, China under Grant KYCX21_2823 and Grant KYCX21_2824.

Data availability Data sharing not applicable to this article as no datasets were generated or analysed during the current study.

Declarations

Conflict of interest The authors declare that they have no conflict of interest.

References

An XL, Qiao S (2021) The hidden, period-adding, mixed-mode oscillations and control in a HR neuron under electromagnetic induction. Chaos Solitons Fractals 143:110587

Bahramian A, Parastesh F, Pham VT, Kapitaniak T, Jafari S, Perc M (2021) Collective behavior in a two-layer neural network with time-varying chemical connections that are controlled by a Petri net. Chaos 31:033138

Bakiri M, Guyeux C, Couchot JF, Marangio L, Galatolo S (2018) A hardware and secure pseudorandom generator for constrained devices. IEEE Trans Ind Informat 14:3754–3765

Bao BC, Xu Q, Bao H, Chen M (2016) Extreme multistability in a memristive circuit. Electron Lett 52:1008–1010

Bao H, Liu WB, Hu AH (2019a) Coexisting multiple firing patterns in two adjacent neurons coupled by memristive electromagnetic induction. Nonlinear Dyn 95:43–56

Bao H, Liu WB, Chen M (2019b) Hidden extreme multistability and dimensionality reduction analysis for improved non-autonomous memristive FitzHugh-Nagumo circuit. Nonlinear Dyn 96:1879–1894

Bao BC, Yang QF, Zhu D, Zhang YZ, Xu Q, Chen M (2020) Initial-induced coexisting and synchronous firing activities in memristor synapse-coupled Morris-Lecar bi-neuron network. Nonlinear Dyn 99:2339–2354

Chay TR (1985) Chaos in a three-variable model of an excitable cell. Physica D 16:233–242

De S, Balakrishnan J (2020) Burst mechanisms and burst synchronization in a system of coupled type-I and type-II neurons. Commun Nonlinear Sci Numer Simul 90:105391

Duarte R, Morrison A (2019) Leveraging heterogeneity for neural computation with fading memory in layer 2/3 cortical microcircuits. PLoS Comput Biol 15:e1006781

Elson RC, Selverston AI, Huerta R, Rulkov NF, Rabinovich MI, Abarbanel HDI (1998) Synchronous behavior of two coupled biological neurons. Phys Rev Lett 81:5692

FitzHugh R (1961) Impulses and physiological states in theoretical models of nerve membrane. Biophys J 1:445–466

Gjorgieva J, Drion G, Marder E (2016) Computational implications of biophysical diversity and multiple timescales in neurons and synapses for circuit performance. Curr Opin Neurobiol 37:44–52

Gosak M, Milojević M, Duh M, Skok K, Perc M (2022) Networks behind the morphology and structural design of living systems. Phys Life Rev 41:1–21

Gu HG, Pan BB, Chen GR, Duan LX (2014) Biological experimental demonstration of bifurcations from bursting to spiking predicted by theoretical models. Nonlinear Dyn 78:391–407

Hodgkin AL, Huxley AF (1990) A quantitative description of membrane current and its application to conduction and excitation in nerve. Bull Math Biol 52:25–71

Lengler J, Jug F, Steger A (2013) Reliable neuronal systems: the importance of heterogeneity. PLoS ONE 8:e80694

Li KX, Bao H, Li HZ, Ma J, Hua ZY, Bao BC (2021a) Memristive Rulkov neuron model with magnetic induction effects. IEEE Trans Ind Inform 18:1726–1736

Li ZJ, Zhou HY, Wang MJ, Ma ML (2021b) Coexisting firing patterns and phase synchronization in locally active memristor coupled neurons with HR and FN models. Nonlinear Dyn 104:1455–1473

Liu ZL, Wang CN, Jin WY, Ma J (2019) Capacitor coupling induces synchronization between neural circuits. Nonlinear Dyn 97:2661–2673

Lv M, Ma J (2016) Multiple modes of electrical activities in a new neuron model under electromagnetic radiation. Neurocomputing 205:375–381

Ma J, Lv M, Zhou P, Xu Y, Hayat T (2017) Phase synchronization between two neurons induced by coupling of electromagnetic field. Appl Math Comput 307:321–328

Majhi S, Perc M, Ghosh D (2022) Dynamics on higher-order networks: A review. J R Soc Interface 19:20220043

Mehrabbeik M, Parastesh F, Ramadoss J, Rajagopal K, Namazi H, Jafari S (2021) Synchronization and chimera states in the network of electrochemically coupled memristive Rulkov neuron maps. Math Biosci Eng 18:9394–9409

Morris C, Lecar H (1981) Voltage oscillations in the barnacle giant muscle fiber. Biophys J 35:193–213

Nakamura O, Tateno K (2019) Random pulse induced synchronization and resonance in uncoupled non-identical neuron models. Cogn Neurodynamics 13:303–312

Njitacke ZT, Koumetio BN, Ramakrishnan B, Leutcho GD, Fozin TF, Tsafack N, Rajagopal K, Kengne J (2021) Hamiltonian energy and coexistence of hidden firing patterns from bidirectional coupling between two different neurons. Cogn Neurodynamics. https://doi.org/10.1007/s11571-021-09747-1

Padmanabhan K, Urban NN (2010) Intrinsic biophysical diversity decorrelates neuronal firing while increasing information content. Nat Neurosci 13:1276–1282

Pal K, Ghosh D, Gangopadhyay G (2020) Synchronization and metabolic energy consumption in stochastic Hodgkin-Huxley neurons: Patch size and drug blockers. Neurocomputing 422:222–234

Parastesh F, Rajagopal K, Jafari S, Perc M, Schöll E (2022) Blinking coupling enhances network synchronization. Phys Rev E 105:054304

Perez-Nieves N, Leung VCH, Dragotti PL, Goodman DFM (2021) Neural heterogeneity promotes robust learning. Nature Commun 12:5791

Pisarchik AN, Feudel U (2014) Control of multistability. Phys Rep 540:167–218

Pisarchik AN, Jaimes-Reátegui R, Garcia-Vellisca MA (2018) Asymmetry in electrical coupling between neurons alters multistable firing behavior. Chaos 28:033605

Sachdeva PS, Livezey JA, DeWeese MR (2020) Heterogeneous synaptic weighting improves neural coding in the presence of common noise. Neural Comput 32:1239–1276

Sar GK, Chowdhury SN, Perc M, Ghosh D (2022) Swarmalators under competitive time-varying phase interactions. New J Phys 24:043004

Semenov DM, Fradkov AL (2021) Adaptive synchronization in the complex heterogeneous networks of Hindmarsh-Rose neurons. Chaos Solitons Fractals 150:111170

Shim Y, Husbands P (2018) The chaotic dynamics and multistability of two coupled Fitzhugh-Nagumo model neurons. Adapt Behave 26:165–176

Wang ZL, Shi XR (2012) Lag synchronization of two identical Hindmarsh-Rose neuron systems with mismatched parameters and external disturbance via a single sliding mode controller. Appl Math Comput 218:10914–10921

Wang H, Lu Q, Shi X (2010) Phase synchronization and its transition in two coupled bursting neurons: theoretical and numerical analysis. Chin Phys B 19:060509

Wang GW, Yu D, Ding QM, Li TY, Jia Y (2021) Effects of electric field on multiple vibrational resonances in Hindmarsh-Rose neuronal systems. Chaos Solitons Fractals 150:111210

Wouapi MK, Fotsin BH, Ngouonkadi EBM, Kemwoue FF, Njitacke ZT (2021) Complex bifurcation analysis and synchronization optimal control for Hindmarsh-Rose model under magnetic flow effect. Cogn Neurodynamics 15:315–347

Wu XY, Ma J, Yuan LH, Liu Y (2014) Simulating electric activities of neurons by using PSPICE. Nonlinear Dyn 75:113–126

Wu FQ, Gao YT, Ma J (2022) Reproduce the biophysical function of chemical synapse by using a memristive synapse. Nonlinear Dyn. https://doi.org/10.1007/S11071-022-07533-0

Xie Y, Yao Z, Ma J (2022) Phase synchronization and energy balance between neurons. Front Inform Technol Electron Eng. https://doi.org/10.1631/FITEE.2100563

Xu Q, Zhu D (2020) FPGA-based experimental validations of electrical activities in two adjacent FitzHugh-Nagumo neurons coupled by memristive electromagnetic induction. IETE Techn Rev 38:563–577

Xu Y, Jia Y, Ge MY, Lu LL, Yang LJ, Zhan X (2017) Effects of ion channel blocks on electrical activity of stochastic Hodgkin-Huxley neural network under electromagnetic induction. Neurocomputing 283:196–204

Xu Q, Tan X, Zhu D, Bao H, Hu YH, Bao BC (2020) Bifurcations to bursting and spiking in the Chay neuron and their validation in a digital circuit. Chaos Soliton Fractals 141:110353

Xu Q, Ju ZT, Ding SK, Feng CT, Chen M, Bao BC (2021a) Electromagnetic induction effects on electrical activity within a memristive Wilson neuron model. Cogn Neurodynamics. https://doi.org/10.1007/s11571-021-09764-0

Xu Q, Liu T, Feng CT, Bao H, Wu HG, Bao BC (2021b) Continuous non-autonomous memristive Rulkov model with extreme multistability. Chin Phys B 30:128702

Yang Y, Liao XF (2019) Filippov Hindmarsh-Rose neuronal model with threshold policy control. IEEE Trans Neural Netw Learning Syst 30:306–311

Yang YM, Ma J, Xu Y, Jia Y (2021) Energy dependence on discharge mode of Izhikevich neuron driven by external stimulus under electromagnetic induction. Cogn Neurodynamics 15:265–277

Yao Z, Zhou P, Zhu ZG, Zhu J (2021) Phase synchronization between a light-dependent neuron and a thermosensitive neuron. Neurocomputing 423:518–534

Yu F, Zhang ZN, Shen H, Huang YY, Cai S, Du SC (2022) FPGA implementation and image encryption application of a new PRNG based on a memristive Hopfield neural network with a special activation gradient. Chin Phys B 31:020505

Zhang JH, Liao XF (2017) Synchronization and chaos in coupled memristor-based FitzHugh-Nagumo circuits with memristor synapse. AEU-Int J Electro Commun 75:82–90

Zhang Y, Wang CN, Tang J, Ma J, Ren GD (2020) Phase coupling synchronization of FHN neurons connected by a Josephson junction. Sci China Technol Sc 63:2328–2338

Zhou P, Zhang XF, Ma J (2022) How to wake up the electric synapse coupling between neurons? Nonlinear Dyn 108:1681–1695